2018

Tuhualite in a Peralkaline Rhyolitic Ignimbrite from Pantelleria, Italy

Boguslaw Baginski
University of Warsaw

Ray Macdonald
Lancaster University

John C. White
Eastern Kentucky University, john.white@eku.edu

Lidia Jezak
University of Warsaw

Recommended Citation

Bagiński, B., Macdonald, R., White, J.C., Jeżak, L., 2018, Tuhualite in a Peralkaline Rhyolitic Ignimbrite from Pantelleria, Italy. European Journal of Mineralogy, v. 30 (2), p. 367-373. (doi: 10.1127/ejm/2018/0030-2711)

Eur J Mineral
PrePub DOI: 10.1127/ejm/2018/0030-2711

PrePub Article

Tuhualite in a peralkaline rhyolitic ignimbrite from Pantelleria, Italy

Bogusław BAGIŃSKI[1,*], Ray MACDONALD[1,2], John C. WHITE[3] and Lidia JEŻAK[1]

[1] Institute of Geochemistry, Mineralogy and Petrology, University of Warsaw, al. Zwirki i Wigury 93, 02-089 Warsaw, Poland
*Corresponding author, e-mail: b.baginski1@uw.edu.pl
[2] Environment Centre, Lancaster University, Lancaster LA1 4YQ, UK
[3] Department of Geosciences, Eastern Kentucky University, Richmond, Kentucky, USA

Abstract: An occurrence of the rare mineral tuhualite ($NaFe^{3+}Fe^{2+}Si_6O_{15}$) is reported in a peralkaline rhyolitic ignimbrite from the island of Pantelleria, Italy. The mineral formed during devitrification of glassy fiamme and varies in form from anhedral plates to perfect euhedral in open vesicles. There is significant replacement of Fe^{2+} by Mn ($\leq$0.37 atoms per formula unit (apfu)) and Zn ($\leq$0.11 apfu), and of Na by K ($\leq$0.13 apfu). The tuhualite possibly formed at temperatures <580 °C at fO_2>FMQ in the presence of a hydrous fluid.

Key-words: tuhualite: peralkaline ignimbrite; Pantelleria; compositional variation; conditions of formation.

1. Introduction

The mineral tuhualite ($NaFe^{3+}Fe^{2+}Si_6O_{15}$) has been recorded from only two localities, in peralkaline rhyolites (~130 ka – present) from the type locality, Mayor Island, New Zealand (Marshall, 1932, 1936), and in a 390–392 Ma peralkaline granite of the Khaldzan Buregtey Massif, Mongolia (Andreeva, 2016). According to mindat.org, it has also been found in pegmatites at Dara i Pioz, Tajikistan, by L.M. Pautov. The scarcity of recorded occurrences is perhaps surprising, in that peralkaline rhyolites and granites are not uncommon lithologies. Furthermore, tuhualite is compositionally rather simple; it has similarities, for example, to aegirine ($NaFe^{3+}Si_2O_6$). The scarcity also means that very little is known about compositional variation in the mineral; only six analyses are available in the literature, four of them published prior to 1970 (Hutton, 1956; Nicholls and Carmichael, 1969; Andreeva, 2016).

Here we report on the occurrence of tuhualite in a peralkaline rhyolitic ignimbrite from the island of Pantelleria, Italy, providing the first substantial analytical data set for the phase. Compositional variations related to differences in textural type, form and colour are assessed and the possible significance of the mineral in the cooling/crystallization history of the ignimbrite is discussed.

2. Geological setting

The island of Pantelleria is located within the continental rift of the Strait of Sicily (Fig. 1). The structure of the island is dominated by two nested calderas (Mahood and Hildreth, 1986), the La Vecchia caldera, dated at 140–146 ka using palaeomagnetic methods and $^{40}Ar/^{39}Ar$ ages (Speranza *et al.*, 2012; Rotolo *et al.*, 2013), and the Cinque Denti (or Monastero) caldera, formed at 45.7 ± 1 ka (2σ) (Scaillet *et al.*, 2013). Formation of the latter caldera was associated with the eruption of the Green Tuff, an ignimbrite showing gradational compositional zoning with height, from pantellerite at the base to comenditic trachyte at the top (Mahood and Hildreth, 1986; Williams *et al.*, 2014). The ignimbrite is a massive, very poorly sorted lapilli tuff with local gradations into diffuse-bedded and block-bearing facies (Williams *et al.*, 2014). As well as rapid lateral variations in thickness, the unit shows rapid vertical and lateral variations in the degree of post-emplacement welding and rheomorphic textures, such that a consistent stratigraphy of the deposit is difficult to establish. Williams *et al.* (2014) used Zr concentration as a proxy for height in the tuff and thus for depth in the pre-eruptive magma reservoir, and established a type section for the tuff at a locality in the western caldera wall (Fig. 1).

3. Analytical methods

The whole-rock analysis (Table 1) was made at Bureau Veritas Commodities Canada Ltd. Major elements and Cr were analysed by inductively coupled plasma–emission spectroscopy, and trace elements, including *REE*, by inductively coupled plasma-mass spectrometry. Mean detection limits on major elements were close to 0.1 wt%, whilst the detection limits for trace elements varied from 0.01 to 0.1 ppm. Mineral compositions were determined

0935-1221/18/0030-2711 $ 3.15
https://doi.org/10.1127/ejm/2018/0030-2711

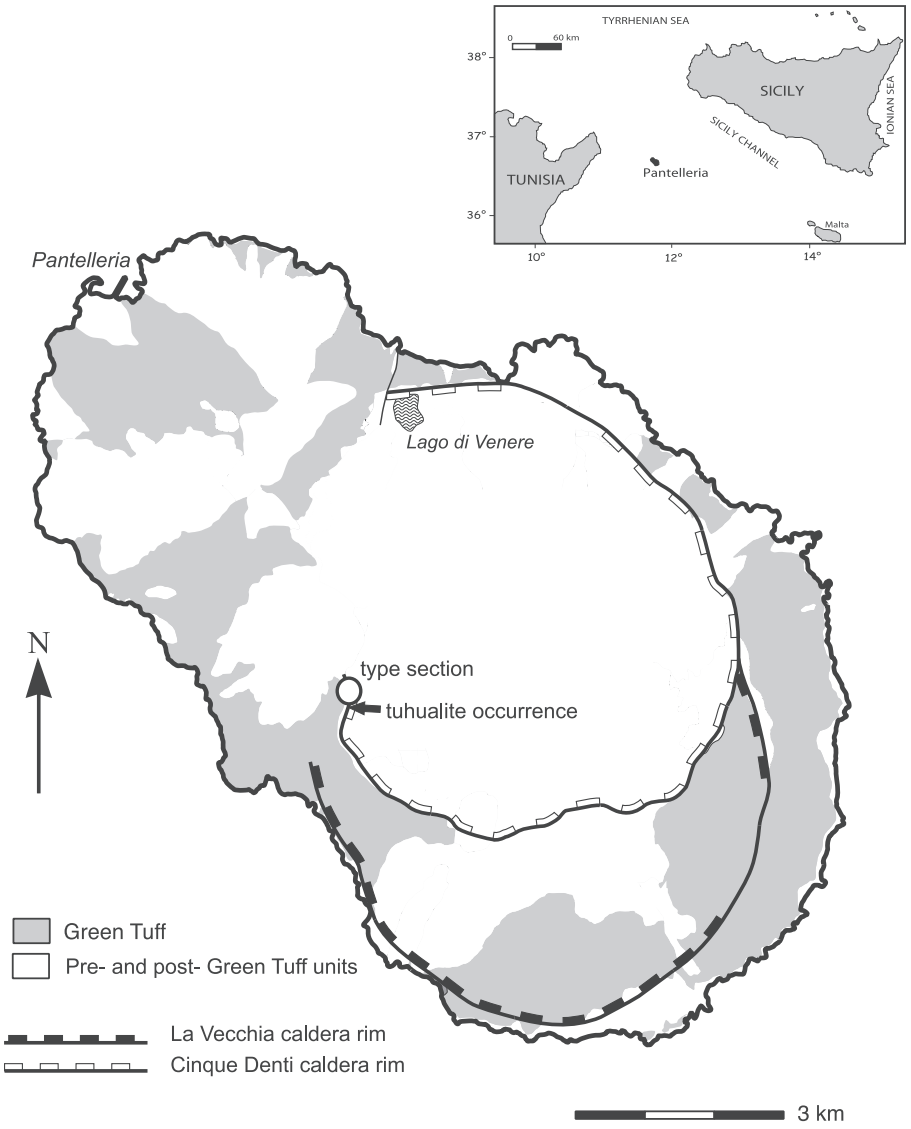

Fig. 1. Distribution of the Green Tuff ignimbrite on Pantelleria. Also shown are the rims of the La Vecchia and Cinque Denti calderas. Much simplified from Scaillet *et al.* (2011). The open circle shows the type section of the Green Tuff proposed by Williams *et al.* (2014), close to the occurrence of the tuhualite-bearing rock.

by electron microprobe at the Inter-Institute Analytical Complex at the Institute of Geochemistry, Mineralogy and Petrology, University of Warsaw, using a Cameca SX-100 microprobe equipped with four wavelength dispersive spectrometers (WDS). The analytical conditions were: accelerating voltage 15 kV and probe current 20–40 nA, with counting times Table A1 of 20 s on peak and 10 s on each of two background positions. The standards, crystals and X-ray lines used, and approximate detection limits are given in Table S1 Table S1 of the Electronic Supplementary Materials. The 'PAP'Φ (ρZ) program of Pouchou and Pichoir (1991) was used for corrections. Chlorine and F were sought on the WDS spectra but were not detected; these halogens were also not found in the Mayor Island tuhualite (Nicholls and Carmichael, 1969).

Formula units of Fe^{3+} in tuhualite (ST1A) were calculated by stoichiometry. The analysis with all Fe as FeO was normalised to 9 cations total and then Fe^{3+} per formula unit was calculated as equal to (15–number of O corresponding to this number of cations) *2 . $Fe^{2+} = Fe^{*} - Fe^{3+}$ (Fe^{*} is measured Fe normalised to 9 cations). Including the calculated Fe_2O_3 and FeO wt.% as input, the analysis can be normalised to 15 oxygens, which should give a total of exactly 9 cations as a check on the method. Even after the recalculation, some oxide totals are low, in the range 98–99 wt%. It is possible that the tuhualite contains some water: Hutton (1956), for example, reported 1.61 wt% H_2O+ in a wet-chemical analysis of the Mayor Island tuhualite, and Merlino (1969) proposed that water molecules occupied channel sites in the mineral. It should be noted, however, that in their optical and IR spectroscopic study of tuhualite, Taran and Rossman (2001) found no absorption bands caused by H_2O or OH stretching vibrations in the mid/near-infrared region. Aegirine formulae (ST1B) were calculated on the basis of 6 oxygens and 4 cations, and amphibole formulae to 8 Si

Table 1. Whole-rock composition.

wt%		ppm		ppm	
SiO_2	69.51	Ba	16	Y	53.1
TiO_2	0.48	Be	6	La	146.6
Al_2O_3	11.39	Co	0.3	Ce	269.7
FeO^*	6.39	Cs	0.3	Pr	26.94
MnO	0.25	Ga	33.9	Nd	92.2
MgO	0.25	Hf	34.4	Sm	14.94
CaO	0.44	Nb	265.5	Eu	1.82
Na_2O	5.08	Rb	145.8	Gd	11.65
K_2O	4.91	Sc	6	Tb	1.81
P_2O_5	0.03	Sn	8	Dy	10.7
LOI	0.2	Sr	2.4	Ho	2.03
Total	98.93	Ta	17.3	Er	6.46
	–	Th	27.4	Tm	1.02
PI	1.20	U	5.2	Yb	7.38
	–	W	1.1	Lu	1.18
	–	Zr	1451.3	–	–

FeO^*, all Fe as Fe^{2+}. PI, Peralkalinity Index (mol. $(Na_2O+K_2O)/Al_2O3$).

and 24 oxygens (ST1B). The contents of Fe^{3+} and Fe^{2+} in both minerals were calculated by stoichiometry as explained above.

Quantitative element distribution maps were acquired in the Cryo-SEM laboratory, Faculty of Geology, University of Warsaw, using a Zeiss Σigma™/VP FE (field emission) – SEM equipped with new generation SDD-type two EDS (XFlash 6/10™) detectors produced by Bruker. An acceleration voltage of 30 kV and a 120 μm aperture were used. EDS electron throughput and X-ray signal amplification were configured to keep the dead time below 8%. 8 × 9 tiles (256 × 196 pixel/12.5 min per tile) were mapped using automatic Bruker Esprit® software.

Although the tuhualite was relatively easily fragmented during thin section preparation, as found by Hutton (1956) for the Mayor Island phase, it was very stable under the electron beam.

4. Occurrence: the host rock

Tuhualite has been found in a densely welded facies of the Green Tuff in the Zighidi section of the Cinque Denti caldera wall (36°46′25.6″N/11°58′28.8″E). The specimen was collected about 2 m above the base of the sheet (Fig. 1). This is the only locality in the tuff where the mineral has so far been found. The host rock is grey-green and densely welded, with strongly flattened fiamme and vesicles (Fig. 2A). There are three types of layers. Type-1 layers are light-green, coarsely vesicular, with alkali feldspar phenocrysts up to 2.2 × 1 mm. The vesicles are stretched parallel to the fiamme. The pale-yellow material rimming an elongated vesicle is a thin coating of Fe ± Mn hydroxide? on quartz and feldspar. Type-2 layer is deep green, microvesicular and carries alkali feldspar crystals up to 2.9 × 1.2 mm. Many of the vesicles are rounded and may represent a phase of post-emplacement degassing. Type-3 layers are light-green and poorly vesicular, with alkali feldspar phenocrysts up to 2 × 0.6 mm. The yellow material is, as in type-1 layers, staining by what is taken to be Fe ± Mn hydroxide. Tuhualite is restricted to the type-1 layer.

Thin sections show that the matrix is largely devitrified into coarser and finer layers (Fig. 3A), carrying alkali feldspar and quartz with smaller amounts of hedenbergite and aenigmatite. Interstitial to alkali feldspar rods are anhedral grains of an unidentified K-Fe-silicate with up to 6 wt% ZrO_2.

5. Occurrence of tuhualite

Violet-coloured tuhualite is seen in the fiamme and, in particular, is associated with the flattened vesicles (Fig. 2B). It is strongly pleochroic, with the scheme α – pale violet, β – violet, γ – dark violet. Locally it is very abundant (Fig. 3A), especially in the more coarsely devitrified layers, although that may partly be a function of it being less easily recognised in the darker, finer layers (Fig. 2B). It forms mainly anhedral patches, up to 200 μm in size. In the vesicles, a common form is as rather elongated ovoids, mimicking the shape of the vesicles (Fig. 3A). In other vesicles, tuhualite crystals grew in from the vesicle wall, often associated with aegirine, amphibole and an unusual skeletal form of alkali feldspar (Fig. 3C and D). Certain vesicles contain perfectly euhedral crystals of tuhualite (Fig. 3B), as reported from the Mayor Island occurrence by Hutton (1956). Commonly the crystals have partial coatings of quartz-feldspar aggregates.

Crystallization of glass in many ash flow tuffs takes place after, or synchronously with, welding (Smith, 1960). Two categories of crystallization seem to have taken place during cooling of the tuhualite-bearing sample: devitrification and vapour-phase crystallization. Devitrification consists of the simultaneous crystallization of alkali feldspar and quartz (or cristobalite) as intergrowths, along with lesser amounts of mafic accessory minerals. The process occurs within the glassy material and can be promoted by late-magmatic fluids. Vapour-phase crystallization is the formation of crystals within pore spaces and is related to the transfer of volatiles. In the Green Tuff, the tuhualite shown in Fig. 3C and D clearly formed in that way. For the crystals in Fig. 3A the situation is less clear. Some occupy vesicles, others form patches and may have formed during devitrification. However, the patches are much larger than the enclosing matrix and may also have precipitated from the vapour phase.

6. Composition of host rock and phenocrysts

Compositionally the host rock is a pantellerite, with a peralkalinity index (PI = mol. $(Na_2O+K_2O)/Al_2O_3$) of 1.20, although that value may have been lowered by some loss of Na during devitrification (Table 1). White *et al.* (2003) introduced the term FK/Al (mol. $(FeO^*+K_2O)/Al_2O_3$, where FeO* is total Fe as Fe^{2+}) as a more robust

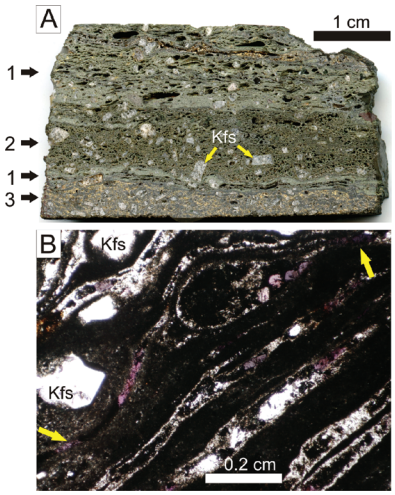

Fig. 2. (A) Photograph of a polished slab of the tuhualite-bearing ignimbrite. Note the layered structure, with layers (numbered) varying in degree of vesicularity and size of alkali feldspar phenocrysts (Kfs). Tuhualite is found only in layer type one. The yellow phase is possibly an Fe ± Mn hydroxide. (B) Photomicrograph of host ignimbrite, with violet tuhualite clearly visible in the coarser, lighter fiamme. It is also present, but less visible, in the darker fiamme: two patches are arrowed. Tuhualite is restricted to type one layers.

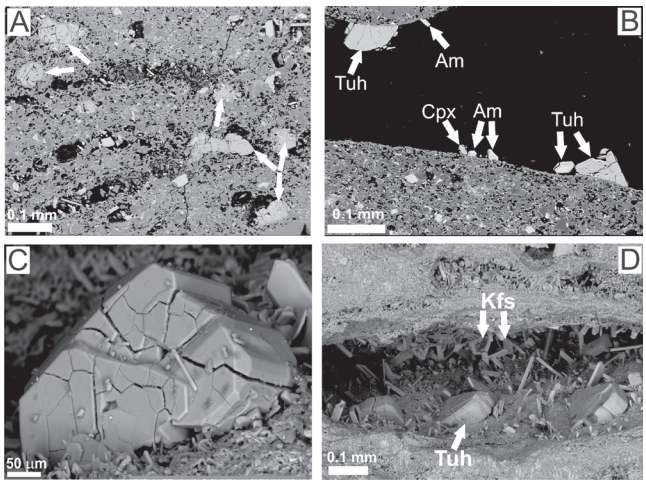

Fig. 3. (A) BSE image, showing tuhualite (Tuh) crystals in both fiamme and pre-welding vesicles in a type one layer. Crystals representing the range of forms have been arrowed. (B) BSE image of tuhualite, sodic amphibole (Am) and aegirine (cpx) projecting from the wall into an empty vesicle. (C) SEM image of euhedral tuhualite in a vesicle. The bright acicular inclusion is aegirine. (D) SEM image of stout euhedral plates of tuhualite and acicular aegirine, sodic amphibole and skeletal alkali feldspar (Kfs) in a vesicle. The tuhualite is embedded in an aggregate of alkali feldspar and quartz.

measure of peralkalinity, in that the components are relatively immobile during devitrification and secondary hydration. The FK/Al value of the ignimbrite is 1.26, which on the basis of an FK/Al – PI regression suggests an original PI of 1.45. The difference between 1.20 and 1.45 corresponds to a Na_2O loss of ~1.7 wt%.

The phenocryst assemblage is alkali feldspar, accompanied by fayalite, hedenbergite and aenigmatite. Ilmenite and apatite occur as inclusions in fayalite and hedenbergite. Alkali feldspar is the dominant phenocryst phase, forming subhedral to euhedral crystals up to ~3 mm across. The total compositional range is $Ab_{64.5–66.3}Or_{33.4–35.5}An_{0–0.4}$; the range within individual crystals is $Or \leq 1$. Aenigmatite occurs as prisms, sometimes slightly rounded, up to 0.68 × 0.38 mm in size. There is a very slight replacement of (Ca+Al) for (Na+Si), namely (Ca+Al = 0.16–0.22 apfu). Fayalite forms partly to heavily resorbed prisms, up to 1.2 × 0.6 × mm in size. The composition is constant at $Fo_{8.3}$. Hedenbergite occurs in several forms, from partly resorbed platy prisms (up to 1 mm across) to anhedral plates. The composition is slightly variable ($Ca_{40.1–43.7}Mg_{9.7–13.1}Fe_{43.1–49.6}$). Ilmenite forms irregular inclusions in fayalite and hedenbergite phenocrysts, with a small compositional range ($X_{ilm} = 0.956–0.969$). Fluorapatite occurs as abundant, zoned inclusions in fayalite and hedenbergite. It is close to the end-member composition, with <2 mol.% britholite component, as judged by the content of (*REE*+Si).

The late-stage pyroxene associated with tuhualite is aegirine of rather variable composition. A crystal forming an inclusion in tuhualite (Fig. 3C) is a titanian variety, with 5.19 wt% TiO_2 ($Na_{0.99}(Fe^{3+}_{0.64}Fe^{2+}_{0.16}Ti_{0.15})_{0.95}Si_{2.00}O_6$). A crystal growing into a vesicle (Fig. 3B) lacks Ti and contains minor Fe^{2+} ($Na_{0.96}(Fe^{3+}_{0.90}Fe^{2+}_{0.09})_{0.99}Si_{1.98}O_6$ (Table S2B). The sodium amphiboles associated with tuhualite in a vesicle (Fig. 3B) are closest to arfvedsonite in composition, but the absence of Fe^{3+}/Fe^{2+}, H_2O, F and Cl determinations precludes calculating structural formulae and identifying the species (Tab. S2B).

No matrix glass survived devitrification, but four glass (melt) inclusions in ilmenite, fayalite and hedenbergite were examined. Robust microprobe analyses were not achieved because of the presence of quench microcrystals and the difficulty in defocussing the electron beam due to the small size of the inclusions. However, the glass is clearly of pantelleritic composition, broadly similar to the whole rock. Chlorine contents of the melt inclusions range from 0.27 to 0.74 (wt%). Assuming that the highest value represents the melt Cl content, the value is consistent with the 1 wt% Cl content estimated from melt inclusions from the inferred, more peralkaline, top of the pre-eruptive magma chamber by Lanzo *et al.* (2013).

6.1. Composition of tuhualite

Representative compositions of the Pantellerian tuhualite are given in Table 2; the complete data set is in Table S2A. The structure of tuhualite consists of six-repeated double chains of silicon tetrahedra and chains of edge-sharing alternating Fe^{2+} tetrahedra and Fe^{3+} octahedra. Sodium atoms are located in six-fold coordination in open structural channels (Merlino, 1969; Taran and Rossman, 2001). In the structural formulae, Fe^{3+} has here been allocated to the octahedral position, and Fe^{2+}, Mn, Mg and Zn to the tetrahedral site. The range of cations in the

Table 2. Representative compositions of tuhualite.

	1	2	3	4	5	6	7	8
Wt%								
SiO_2	65.39	65.75	66.03	65.47	66.53	65.73	66.10	65.21
TiO_2	0.08	bd	bd	0.11	bd	bd	0.09	bd
Al_2O_3	0.07	0.06	bd	0.10	0.05	bd	0.20	0.14
Fe_2O_3	16.62	15.31	15.80	15.79	17.11	15.18	16.83	2.43
FeO	5.48	8.66	6.87	5.51	3.83	6.98	7.75	23.22
MnO	3.30	2.49	3.34	4.83	4.16	3.54	2.15	3.07
ZnO	0.65	0.63	0.76	0.83	0.77	1.17	0.77	0.75
MgO	0.26	0.13	0.30	0.30	0.41	0.10	0.09	0.09
CaO	0.10	bd	bd	0.10	0.12	0.07	0.08	0.05
Na_2O	6.11	5.82	5.78	5.73	6.41	5.36	5.85	1.40
K_2O	0.22	0.10	0.38	0.21	0.11	0.85	0.41	2.06
Total	98.28	98.95	99.26	98.98	99.50	98.98	100.32	98.42
Formulae on basis of 15 oxygens and 9 cations								
Si	5.973	5.992	5.991	5.964	5.983	6.002	5.947	6.158
Ti	0.005	0.000	0.000	0.008	0.000	0.000	0.006	0.000
Al.	0.008	0.006	0.000	0.011	0.005	0.000	0.021	0.016
Fe^{3+}	1.143	1.050	1.079	1.083	1.158	1.043	1.048	0.172
Fe^{2+}	0.419	0.660	0.521	0.420	0.288	0.533	0.679	1.834
Mn	0.255	0.192	0.257	0.373	0.317	0.274	0.164	0.246
Zn	0.044	0.042	0.051	0.056	0.051	0.079	0.051	0.052
Mg	0.035	0.018	0.041	0.041	0.055	0.014	0.012	0.013
Ca	0.010	0.000	0.000	0.010	0.012	0.007	0.008	0.005
Na	1.082	1.028	1.017	1.012	1.118	0.949	1.020	0.256
K	0.026	0.012	0.044	0.024	0.013	0.099	0.047	0.250
Oxid. ratio	0.73	0.61	0.67	0.72	0.80	0.66	0.61	0.09

Explanation: numbers 1, 2, partly fragmented subhedral prism; 3, fragmented rhomb; 4, 5, anhedral plate; 6, ovoidal plate; 7, fractured anhedral plate; 8, dark altered area in ovoidal crystal (Fig. 5) bd, below detection. Oxid. Ratio, oxidation ratio ($Fe^{3+}/(Fe^{3+}+Fe^{2+})$) Fe_2O_3, FeO, Fe^{3+} and Fe^{2+} calculated from stoichiometry (see explanation in text).

octahedral site is 0.96–1.15 apfu (average 1.06 apfu), that in the tetrahedral site is 0.76–1.00 apfu (average 0.88 apfu). The deficiency could be at least partly compensated by allocating some Fe^{3+} to the tetrahedral site.

The analyses include high Mn contents ($\leq$0.37 apfu; 4.83 wt% MnO; Fig. 4A), with $Fe^{2+}/(Fe^{2+}+Mn)$ ratios as low as 0.51. Zinc levels, also significant ($\leq$0.11 apfu; 1.59 wt% ZnO), show no correlation with Fe^{2+} (Fig. 4B). Magnesium values are up to 0.06 apfu (0.41 wt% MgO) and there is a scattered negative correlation with Fe^{2+} (Fig. 4C). Potassium abundances are significant ($\leq$0.13 apfu; 1.03 wt% K_2O; Fig. 4D) and Na/(Na+K) ratios range from 0.88 to 1.0 (excepting altered zones – see below). There is a large composition gap between the most potassic composition and that of a blue, K-rich, variety of tuhualite recorded by Nicholls and Carmichael (1969) from Mayor Island (Na/(Na+K) 0.53).

Compositional variations within crystals are relatively modest; in the crystal shown in Fig. 5, for example, Na ranges from 0.97 to 1.12 apfu and Mn from 0.17 to 0.25 apfu, with no systematic variation related to position within the crystal. Whereas the majority of crystals show no signs of alteration, some crystals show small altered zones. The crystal in Fig. 5, for example, has a central area which, while indistinguishable on standard BSE images, can be seen on element distribution maps of Na and K to have gained K and lost Na (Table 2, no. 8; Table S2A: nos. 98 and 99). Other point analyses indicating K gain and Na loss are in Table S2A, nos. 111–113. It may be that the alkali exchange was related to interaction with late hydrous fluids.

7. Conditions of formation

Textural evidence indicates that the tuhualite formed during the post-magmatic stages. The vesicular nature of the rock reflects the volatile-rich nature of the erupting magma. The stretching of vesicles parallel to the fiamme during welding indicates that the vesicles existed before devitrification of the glassy fiamme began. The presence of tuhualite in both the fiamme and vesicles indicates that it formed during devitrification.

Some constraints on the formation conditions of the host rock are provided by the experimental data of Di Carlo et al. (2010) on a pantellerite from Pantelleria, which is compositionally broadly similar to the Green Tuff. They found that the phenocryst assemblage alkali feldspar + aenigmatite + hedenbergite last equilibrated at $<$700 °C and $\sim$120 MPa, with $fO_2 \sim$ FMQ. Tentatively, they drew the solidus extending from 660 °C at 2.6 wt% melt water to 680 °C at 0 wt% melt water. The temperature of the Green Tuff on eruption may, therefore, have been between 700 and 660 °C.

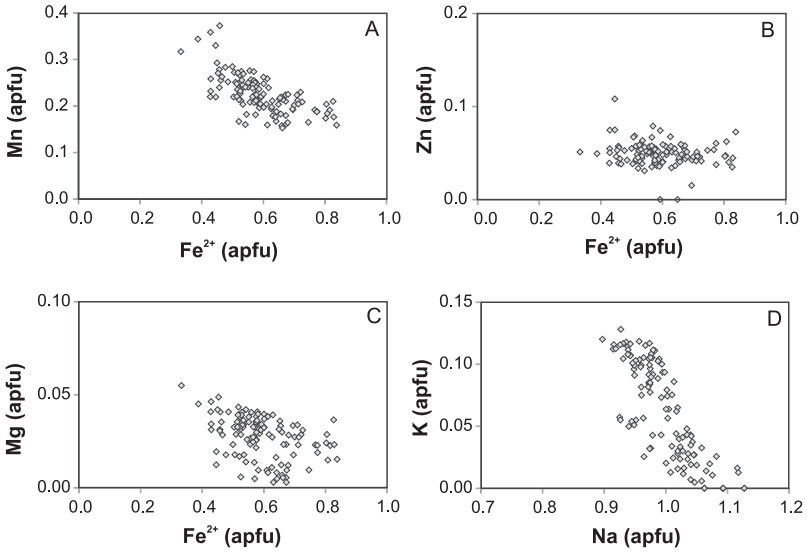

Fig. 4. Plots of Mn (A), Zn (B) and Mg (C) against Fe^{2+} for tuhualite. (D) Na plotted against K. Analyses of K-rich, Na-poor regions in altered crystals have been omitted from (D). Data from Table S2A.

The temperature at which devitrification occurred is more difficult to constrain. One approach is to consider the glass transition temperature (T_g), below which welding of the matrix glass cannot take place. Di Genova *et al.* (2013) have shown that T_g for pantelleritic magmas are low, varying from 520 °C for anhydrous liquids to 402 °C with 1 wt% melt water content. However, T_g is lowered considerably by both water and Cl and these temperatures may well be maximum estimates. The assemblage aenigmatite + aegirine in the absence of Fe-Ti oxides suggests crystallization conditions within the "no-oxide" field of Nicholls and Carmichael (1969). This field is bounded at the lower temperature end by its intersection with the field of hydroxyl-soda amphibole (Ernst, 1962; Vilalva *et al.*, 2016). The rare amphibole in the Pantellerian rock is assumed to be approximated by arfvedsonite. The relationship tuhualite-aegirine-arfvedsonite could be described as:

$$\underset{\text{aegirine}}{NaFe^{3+}Si_2O_6} + 2\underset{\text{tuhualite}}{NaFe^{2+}Fe^{3+}Si_6O_{15}} + H_2O = \underset{\text{arfvedsonite}}{NaNa_2(Fe^{3+}Fe_4^{2+})Si_8O_{22}(OH)_2} + 6SiO_2 + 0.5O_2. \quad (8)$$

This suggests that arfvedsonite would be favoured under higher water fugacities and more reducing conditions (and possibly lower silica activities). However, textural evidence in the Green Tuff seems to indicate that, at least during vapour phase crystallization, the three phases coexisted (Fig. 3B), implying a set of very specific P-T-fluid composition conditions.

The relatively high $Fe^{3+}/(Fe^{3+}+Fe^{2+})$ values in tuhualite and aegirine may suggest oxidizing conditions above FMQ (Bailey, 1969; Marks *et al.*, 2003; Vilalva *et al.*, 2016). However, this ratio is also strongly influenced by melt composition, tending to increase with alkali content (Carmichael and Nicholls, 1967; Sack *et al.*, 1980; Tangeman *et al.*, 2001). A similar effect for Eu^{3+}/Eu^{2+} was documented by White *et al.* (2003). Thus, it is possible to have high oxidation ratios despite the reducing conditions of these fluids suggested by Di Carlo *et al.* (2010).

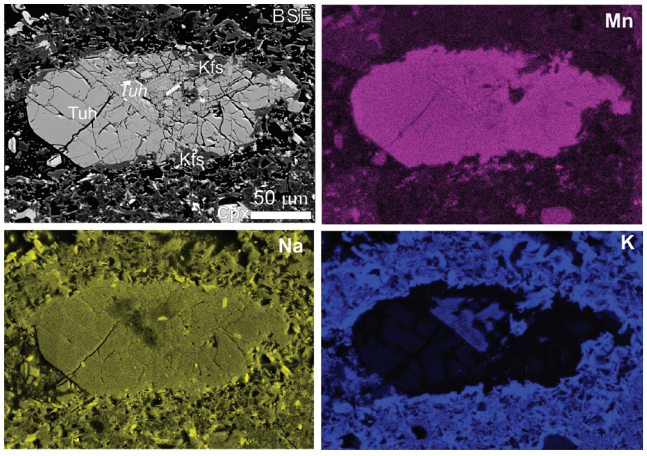

Fig. 5. BSE image and element distribution maps for a partially altered tuhualite crystal. Note, the inverse relationship between Na and K, probably due to interaction with low-temperature fluids. The bright inclusions are aegirine. Data from ST1A, nos. 81–99.

If the interpretation of the small round vesicles in the tuff as due to post-emplacement degassing is correct, it may be that the formation of the tuhualite occurred in the presence of a hydrous fluid. It may not be a coincidence that the most intense staining of the quartz and feldspar occurred in the non-vesicular type-3 layer (Fig. 2); water did not degas there but was trapped and caused the staining.

How do the formation conditions of tuhualite in the Green Tuff compare with the occurrences at Mayor Island and Khaldzan Buregtey? According to Nicholls & Carmichael (1969), tuhualite is generally present in crystalline Mayor Island pantellerites as small interstitial patches with only rare larger euhedral crystals. They suggested that the mineral formed, in association with sodic pyroxenes and amphiboles, as a late magmatic phase. Insufficient information was

given to be able to judge the nature of the interstitial patches, but they may be similar to those shown in Fig. 3A. The euhedral crystals may be comparable to those reported by Hutton (1956) and thus correspond to the euhedral crystals in Fig. 3C. The mode of formation of the Mayor Island tuhualite may, therefore, have been similar to that in the Green Tuff, namely from devitrification and vapour phase crystallization.

The mode of occurrence of tuhualite in the Khaldzan Buregtey alkali granite is uncertain: in (2016, p. 464), it is said to occur as crystalline inclusions in quartz but in Table 2 it is also listed as a major mineral of the rock. The mineral is found in the quartz crystals as rhomb-shaped inclusions ranging from 30 to 40 μm in size, associated with inclusions of potassic feldspar, albite, titanite, fluorite, zircon, gittinsite, pyrochlore and parisite. Andreeva (2016) mentioned the possibility that the tuhualite was of magmatic crystallization. Whatever the mode of formation, it is clearly in a different paragenesis to the Green Tuff and Mayor Island occurrences.

The following questions arise: why are reports of tuhualite apparently so rare globally? Why is it apparently restricted to one locality in the intensively studied Green Tuff? Perhaps it has simply been overlooked but its colour in thin section makes it very distinctive, as already noted by Hutton (1956). Pantelleritic ignimbrites have been recorded from many localities, including the Fantale volcano, Ethiopia (Gibson, 1970), the Late Miocene sequence of central Kenya (Claessens *et al.*, 2016), Gran Canaria (Schmincke, 1969), and the Gold Flat ash flow tuff, Nevada (Noble, 1965). In some cases, the rocks are just as compositionally evolved as the Pantellerian rhyolites and contain comparable mafic phenocryst assemblages (aenigmatite + sodic pyroxene ± amphibole). The crystallization conditions inferred here for the tuhualite-bearing rock are not unusual for pantellerites elsewhere. For example, broadly comparable conditions were found experimentally for pantellerites from the Kenya Rift Valley (Scaillet and Macdonald, 2006). If, as Nicholls and Carmichael (1969) suggested, the tuhualite-bearing assemblage is part of a natural crystallization progression, why has it not been observed more often?

Acknowledgement: The work was supported through the Innovative Economy Operational Program POIG.02.02.00-00-025/09 (NanoFun; Cryo-SEM microscopy lab). We thank Silvio Rotolo, an anonymous reviewer and the handling Associate Editor, Edward S. Grew for constructive, insightful comments on the manuscript, and helpful advice on mineral formulae calculations.

References

Andreeva, I. (2016): Genesis and mechanisms of formation of rare-metal peralkaline granites of the Khaldzan Buregtey Massif, Mongolia: evidence from melt inclusions. *Petrology*, **24**, 462–476.

Bailey, D.K. (1969): The stability of acmite in the presence of water. *Am. J. Sci*., **267-A**, 1–16.

Carmichael, I.S.E. & Nicholls, J. (1967): Oxides and oxygen fugacities in volcanic rocks. *J. Geophys. Res*., **72**, 4665–4687.

Claessens, L., Veldkamp, A., Schoorl, J.M., Wijbrans, J.R., Van Gorp, W., Macdonald, R. (2016): Large scale pantelleritic ash flow eruptions during the Late Miocene in central Kenya and evidence for significant environmental impact. *Global Planet. Change*, **145**, 30–41.

Di Carlo, I., Rotolo, S.G., Scaillet, B., Buccheri, V., Pichavant, M. (2010): Phase equilibrium constraints on pre-eruptive conditions of recent felsic explosive volcanism at Pantelleria Island, Italy. *J. Petrol.*, **51**, 2245–2276.

Di Genova, D., Romano, C., Hess, K.-U., Vona, A., Poe, B.T., Giordano, D., Dingwell, D.B., Behrens, W. (2013): The rheology of peralkaline rhyolites from Pantelleria Island. *J. Volcanol. Geotherm. Res*., **249**, 201–216.

Ernst, W.G. (1962): Synthesis, stability relations and occurrence of riebeckite-arfvedsonite solid solutions. *J. Geol*., **70**, 689–736.

Gibson, I.L. (1970): A pantelleritic welded ash-flow from the Ethiopian Rift Valley. *Contrib. Mineral. Petrol*., **28**, 89–111.

Hutton, C.O. (1956): Re-examination of the mineral tuhualite. *Mineral. Mag*., **31**, 96–106.

Lanzo, G., Landi, P., Rotolo, S.G. (2013): Volatiles in pantellerite magmas: a case study of the Green Tuff Plinian eruption (Island of Pantelleria, Italy). *J. Volcanol. Geotherm. Res.*, **262**, 153–163.

Mahood, G.A. & Hildreth, W. (1986): Geology of the peralkaline volcano at Pantelleria, Strait of Sicily. *Bull. Volcanol.*, **48**, 143–172.

Marks, M., Vennemann, T., Siebel, W., Markl, G. (2003): Quantification of magmatic and hydrothermal processes in a syenite-alkali granite complex based on temperatures, phase equilibria, and stable and radiogenic isotopes. *J. Petrol*., **44**, 1247–1280.

Marshall, P. (1932): Notes on some volcanic rocks of the North Island of New Zealand. *N. Z. J. Sci. Technol*., **13**, 201.

— (1936): The mineral tuhualite. *Trans. R. Soc. N. Z.*, **66**, 330–336.

Merlino, S. (1969): Tuhualite crystal structure. *Science*, **166**, 1399–1401.

Nicholls, J. & Carmichael, I.S.E. (1969): Peralkaline acid liquids: a petrological study. *Contrib. Mineral. Petrol*., **20**, 268–294.

Noble, D.C. (1965): Gold Flat Member of the Thirsty Canyon Tuff − a pantelleritic ash-flow tuff sheet in southern Nevada. U.S. *Geol. Surv. Prof. Pap.*, **525-B**, B85– B90.

Pouchou, J.L. & Pichoir, J.F. (1991): Quantitative analysis of homogeneous or stratified microvolumes applying the model 'PAP'. *in* "Electron Probe Quantitation" K.F.J. Heinrich & D.E. Newbury, eds., Plenum Press, New York, 31–75.

Rotolo, S.G., Scaillet, S., La Felice, S., Vita-Scaillet, G. (2013): A revision of the structure and stratigraphy of pre-Green Tuff ignimbrites at Pantelleria (Strait of Sicily). *J. Volcanol. Geotherm. Res*., **250**, 61–74.

Sack, R.O., Carmichael, I.S.E., Rivers, M., Ghiorso, M.S. (1980): Ferric-ferrous equilibria in natural silicate liquids at 1 bar. *Contrib. Mineral. Petrol*., **75**, 369–376.

Scaillet, B. & Macdonald, R. (2006): Experimental constraints on pre-eruption conditions of pantelleritic magmas: evidence from the Eburru complex, Kenya Rift. *Lithos*, **91**, 95–108.

Scaillet, S., Rotolo, S.G., La Felice, S., Vita-Scaillet, G. (2011): High-resolution $^{40}Ar/^{39}Ar$ chronostratigraphy of the post-caldera (<20 ka) volcanic activity at Pantelleria, Sicily Strait. *Earth Planet. Sci. Lett*., **309**, 280–290.

Scaillet, S., Vita-Scaillet, G., Rotolo, S.G. (2013): Millenial-scale phase relationships between ice-core and Mediterranean marine records: insights from high-precision $^{40}Ar/^{39}Ar$ dating of the Green Tuff of Pantelleria, Sicily Strait. *Quat. Sci. Rev.*, **78**, 141–154.

Schmincke, H.U. (1969): Ignimbrite sequence on Gran Canaria. *Bull. Volcanol*., **33**, 1199–1219.

Smith, R.L. (1960): Zones and zonal variations in welded ash flows. *U.S. Geol. Surv. Prof. Paper*, **354-F**, 149–159.

Speranza, F., Di Chiara, A., Rotolo, S.G. (2012): Correlation of welded ignimbrites on Pantelleria, using paleomagnetism. *Bull. Volcanol*., **74**, 341–357.

Tangeman, J.A., Lange, R., Forman, L. (2001): Ferric-ferrous equilibria in K_2O-FeO-Fe_2O_3-SiO_2 melts. *Geochim. Cosmochim. Acta*, **65**, 1809–1819.

Taran, M.N. & Rossman, G.R. (2001): Optical spectroscopic study of tuhualite and a re-examination of the beryl, cordierite, and osumilite spectra. *Am. Mineral*., **86**, 973–980.

Vilalva, F.C.J., Vlach, S.R.F., Simonetti, A. (2016): Chemical and O-isotope compositions of amphiboles and clinopyroxenes from A-type granites of the Papanduva Pluton, South Brazil: Insights into late- to post-magmatic evolution of peralkaline systems. *Chem. Geol.*, **420**, 186–199.

White, J.C., Holt, G.S., Parker, D.F., Ren, M. (2003): Trace-element partitioning between alkali feldspar and peralkaline quartz trachyte to rhyolite magma. Part I. Systematics of trace-element partitioning. *Am. Mineral.*, **88**, 316–329.

Williams, R., Branney, M.J., Barry, T.L. (2014): Temporal and spatial evolution of a waxing then waning catastrophic density current revealed by chemical mapping. *Geology*, **42**, 107–110.

Received 3 August 2017
Modified version received 22 November 2017
Accepted 22 November 2017